Superresolution of three-dimensional optical imaging by use of evanescent waves

Patrick C. Chaumet, Kamal Belkebir, and Anne Sentenac

*Institut Fresnel, Centre National de la Recherche Scientifique, Unité Mixte de Recherche (UMR 6133), Campus de Saint Jérôme,
Case 162, Université d'Aix-Marseille I & III, 13397 Marseille Cedex, France*

We simulate a three-dimensional optical diffraction tomography experiment in which superresolution is achieved by illuminating the object with evanescent waves generated by a prism. We show that accounting for multiple scattering between the object and the prism interface is mandatory to obtain superresolved images. Because the Born approximation leads to poor results, we propose a nonlinear inversion method for retrieving the map of permittivity of the object from the scattered far field. We analyze the sensitivity to noise of our algorithm and point out the importance of using incident propagative waves together with evanescent waves to improve the robustness of the reconstruction without losing the superresolution. © 2004 Optical Society of America

OCIS codes: 180.6900, 110.6960, 290.3200.

There has been considerable interest in the development of optical microscopes with lateral resolution below the usual Rayleigh criterion, $\lambda/(2\mathrm{NA})$, where λ is the wavelength of the illumination and NA is the numerical aperture of the imaging system. The resolution has been improved well below the classical limit in optical near-field microscopy[1] by bringing a probe within a few nanometers of the sample. In far-field fluorescence microscopy an important amelioration has been obtained by taking advantage of nonlinear effects[2] or by use of numerical postprocessing with strong prior information on the fluorescent sources. In classical far-field microscopes the NA has been increased with immersed lenses, hemispherical prisms,[3] or the placement of several objectives on opposite sides of the sample.[4,5] It has also been proposed to illuminate the sample with many structured illuminations and to mix the different images through simple arithmetics.[6] This last technique is, in principle, close to optical diffraction tomography (ODT), in which the sample is illuminated under various angles of incidence, the phase and intensity of the diffracted far-field is detected along several directions of observation,[7] and a numerical procedure is used to retrieve the map of permittivity of the object from the far-field data.[8] In general, the inversion methods are based on the Born approximation, so that there is a linear relationship between the scattered field and the permittivity of the object.[9] Experimental and theoretical studies have shown that using several illuminations permits one to exceed the classical diffraction limit by a factor of 2.[6,8] To ameliorate further the resolution of the system, it has been proposed to illuminate the sample with evanescent waves through a prism in total internal reflection.[10] Actually, superresolution is obtained if the objects are close to the surface of the prism or even deposited onto it.[11] In this case the influence of the interface cannot be neglected, as was done in the pioneering work on this technique.[10] In this Letter we simulate accurately a full-vectorial three-dimensional

ODT experiment in total internal reflection configuration. We point out that multiple scattering between the object and the interface is not negligible. Hence, contrary to what happens for configurations without an interface, the Born approximation leads to nonsatisfactory results even for objects that are small with respect to the wavelength. We thus propose a full-vectorial nonlinear inversion method and investigate its power of resolution. Last, we show that the robustness of the reconstruction with respect to noise can be significantly increased by use of both propagative- and evanescent-wave illumination beams.

The geometry of the problem is depicted in Fig. 1. Assume that an unknown three-dimensional object is entirely confined in a bounded box $\Omega \subset \mathbb{R}^3$ (investigation domain) and illuminated successively by $l = 1, \ldots, L$ electromagnetic waves $\mathbf{E}^{\mathrm{inc}}_{l=1,\ldots,L}$. For each excitation l the scattered field $\mathbf{f}_l$ is measured at M points on a surface Γ located outside the investigation domain Ω. We use the coupled dipole method
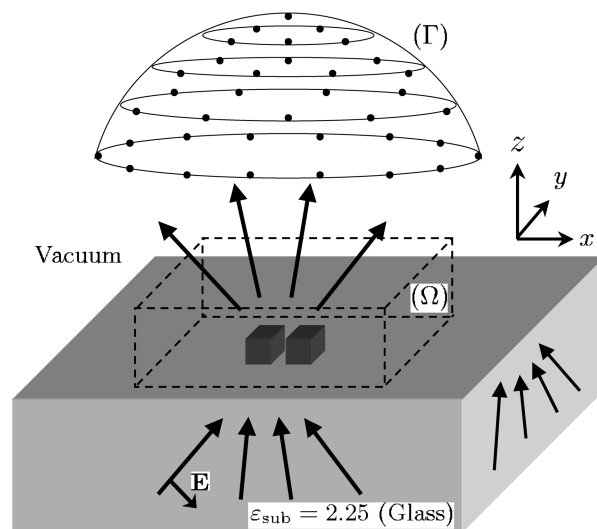

Fig. 1.   Sketch of the ODT experiment.

(CDM) to model the scattered field by an arbitrary three-dimensional object deposited on a semi-infinite medium.[12] In this method the scatterer is discretized into a cubic lattice of N subunits with spacing d that are considered radiating dipoles. The self-consistent local field at a subunit i inside Ω can be written as

$$\mathbf{E}_l(\mathbf{r}_i \in \Omega) = \mathbf{E}_l^{\mathrm{inc}}(\mathbf{r}_i) + \sum_{j=1}^{N} \overset{\leftrightarrow}{\mathbf{G}}(\mathbf{r}_i, \mathbf{r}_j)\alpha(\mathbf{r}_j)\mathbf{E}_l(\mathbf{r}_j), \quad (1)$$

where $\overset{\leftrightarrow}{\mathbf{G}}$ is the field susceptibility tensor that takes into account the substrate[12] and $i = 1, \ldots, N$. $\alpha(\mathbf{r}_j)$ denotes the polarizability of subunit j depending on d through the Clausius–Mossotti relation.[12] The scattered field on Γ reads as

$$\mathbf{E}_l^d(\mathbf{r}_m \in \Gamma) = \sum_{j=1}^{N} \overset{\leftrightarrow}{\mathbf{G}}(\mathbf{r}_m, \mathbf{r}_j)\alpha(\mathbf{r}_j)\mathbf{E}_l(\mathbf{r}_j). \quad (2)$$

For each illumination the forward scattering problem, Eqs. (1) and (2), can be reformulated symbolically as

$$\mathbf{E}_l^d = \overline{\overline{\mathbf{G}}}_{\mathrm{far}}\alpha\mathbf{E}_l, \quad (3)$$

$$\mathbf{E}_l = \mathbf{E}_l^{\mathrm{inc}} + \overline{\overline{\mathbf{G}}}_{\mathrm{near}}\alpha\mathbf{E}_l, \quad (4)$$

where $\overline{\overline{\mathbf{G}}}_{\mathrm{far}}$ and $\overline{\overline{\mathbf{G}}}_{\mathrm{near}}$ are matrices that contain the field susceptibility tensor and are $(3N \times 3M)$ and $(3N \times 3N)$, respectively. The inverse scattering problem consists of finding the permittivity distribution ε inside investigation area Ω such that the associated scattered field matches measured field $\mathbf{f}_{l=1,\ldots,L}$. To solve this nonlinear and ill-posed inverse scattering problem, we propose an iterative approach as described for the two-dimensional case in Ref. 13. In this approach, starting from an initial guess, the parameter of interest (the polarizability distribution and subsequently the permittivity) is adjusted gradually by minimizing a cost functional $\mathcal{F}(\alpha)$ involving the discrepancy between the data $\mathbf{f}_l$ and the scattered field that is predicted by the model through Eqs. (3) and (4). In fact, the inverse problem is stated as an optimization problem in which for each iteration step n the cost functional

$$\mathcal{F}_n(\alpha_n) = \sum_{l=1}^{L} \|\mathbf{f}_l - \overline{\overline{\mathbf{G}}}_{\mathrm{far}}\alpha_n\mathbf{E}_{l,n}\|_\Gamma^2 \Big/ \sum_{l=1}^{L} \|\mathbf{f}_l\|_\Gamma^2 \quad (5)$$

is minimized by the Polak–Ribière conjugate gradient procedure as in Ref. 13. When the extended Born approximation[14] is assumed, local field $\mathbf{E}_l$ is approximated by incident field $\mathbf{E}_l^{\mathrm{inc}}$. When multiple scattering is taken into account, local field $\mathbf{E}$ is the solution of Eq. (4) for the best available estimation of the polarizability distribution, i.e.,

$$\mathbf{E}_{n,l} = \left[\overline{\overline{\mathbf{I}}} - \overline{\overline{\mathbf{G}}}_{\mathrm{near}}\alpha_{n-1}\right]^{-1}\mathbf{E}_l^{\mathrm{inc}}, \quad (6)$$

with $\overline{\overline{\mathbf{I}}}$ being the identity matrix.

We check the performance of the inverse procedure on synthetic data by simulating an ODT experiment with the CDM. Consider two cubes of side $\lambda/4$ and of relative permittivity 2.25 separated by $\lambda/10$, deposited on a semi-infinite medium with a relative permittivity of $\varepsilon_{\mathrm{sub}} = 2.25$ (as depicted in Fig. 1). The superstrate is a vacuum, whereas the substrate is made of glass. The object is illuminated by 16 plane waves coming from the substrate, whose wave vectors and electric field are either in the (x, z) plane or in the (y, z) plane. Let θ_l^{inc} be the angle of incidence with respect to the z axis corresponding to the lth illumination. For the total internal reflection experiment, all the incident plane waves are totally reflected at the interface; hence $\theta_l^{\mathrm{inc}} \in [-80, -43] \bigcup [80, 43]$ deg. The amplitude and phase of the scattered fields are detected at 65 points regularly distributed on a half-sphere Γ (see Fig. 1). The radius of the sphere is 400λ so that only data from far-field components are considered. Azimuthal angle of observation θ, defined as the angle between the diffracted wave vector and the z axis, ranges from $-80°$ to $80°$. In all the examples the synthetic data are computed with a mesh size of $\lambda/40$, which differs from that used in the inversion, $\lambda/20$. In all the reported results we display the map of the reconstructed relative permittivity distribution after enough iterations for the cost function to reach a plateau. During the minimization process the value of the relative permittivity was enforced not to exceed 2.25; thus the convergence was obtained within 100 iterations. We first investigate the efficiency of the extended Born approximation[14] (worse results were obtained with the standard Born approximation). In Figs. 2(a) and 2(b) we plot the top and side views of the reconstructed relative permittivity in the (x, y) and (x, z) planes with the linear inversion method. We observe that the two cubes are not resolved and that the relative permittivity quickly saturates at 2.25, especially in the vicinity of the interface. This result can be explained easily by studying the behavior of the local field inside a small dielectric sphere placed above a substrate and illuminated under normal incidence in transmission. When the distance between the object and the interface tends to zero, the amplitude of the local field increases and departs from the transmitted incident field. Thus, although the extended Born approximation underestimates the local
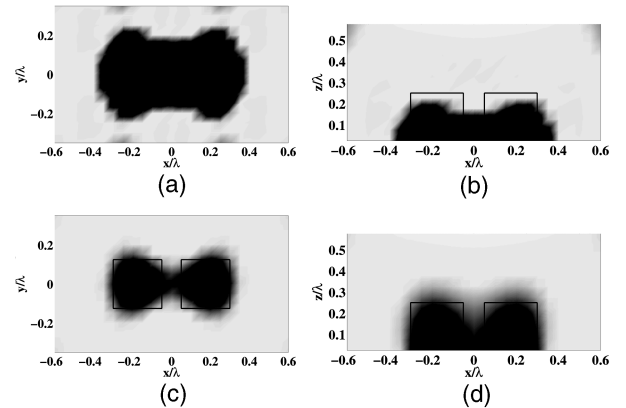

Fig. 2. Reconstructed relative permittivity distribution with only evanescent-wave illumination: (a), (b) with the extended Born approximation; (c), (d) with the nonlinear inverse scheme.
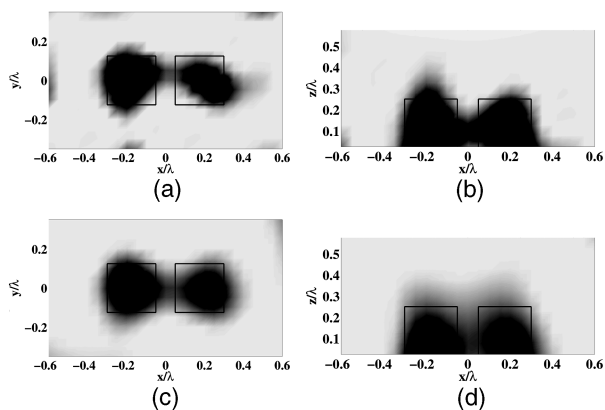
Fig. 3. Reconstructed relative permittivity distribution with the nonlinear inverse algorithm from corrupted data with noise: (a), (b) with evanescent waves; (c), (d) with evanescent and propagative waves.

field, the inversion method compensates this error by overestimating the polarizability of the dipoles close to the interface. The failure of the linear inversion method is clearly due to the presence of the interface. Indeed, we checked the linear inversion method with the same two cubes separated by $\lambda/7$ and illuminated by propagative plane waves only. When objects are deposited on the interface, the reconstructed map of the permittivity is similar to that obtained in Figs. 2(a) and 2(b), whereas, when the objects are in vacuum, they are correctly resolved. Hence it is mandatory to account for the multiple scattering between the objects and the interface in the inverse problem. In Figs. 2(c) and 2(d) we plot the maps of the relative permittivity obtained by taking into account the multiple scattering effect, i.e., the self-consistent Eq. (4) for the local field is solved at each iteration step. The improvement in the resolution and accuracy is manifest. The ability to resolve two cubes separated by $\lambda/10$ is due to both the nonlinear inversion method that accounts for the multiple scattering and the set of incident evanescent plane waves that maximizes the radius of the Ewald sphere that can be covered in such a configuration.[11] When only propagative waves are used, i.e., $\theta_l^{\mathrm{inc}} \in [-43, 43]$ deg, the two cubes are not resolved.

In Fig. 3 we checked the robustness of the inverse method by adding an uncorrelated noise to the scattered far-field data. The noise amplitude is 20% of the maximum of the scattered field for all the illuminations. We note, by comparing Figs. 3(a) and 3(b) with Figs. 2(c) and 2(d), that the reconstructed map of the permittivity is strongly affected by the noise. The same algorithm, used in a homogeneous configuration, shows a better robustness to noise. In our opinion this is because the incident waves that illuminate the objects are evanescent. Indeed, the convergence of iterative inverse schemes deteriorates when the frequency of the illumination is increased.[15] Now, one can consider evanescent waves as high-frequency illumination. It is possible to circumvent the sensitivity

of the reconstruction to noise by using both evanescent and propagative waves as illumination. Indeed, it has been shown that low-frequency illumination, although yielding poorly resolved images, ameliorates the convergence of iterative inversion schemes.[15] In Figs. 3(c) and 3(d) we plot the reconstructed map of the permittivity obtained when $\theta_l^{\mathrm{inc}} \in [-80, 80]$ deg is used to build the set of data. This result has to be compared with Figs. 3(a) and 3(b), in which only evanescent waves are used. The robustness of the inversion algorithm is clearly improved. Note that the resolution is not deteriorated by the use of propagative waves together with evanescent waves.

In conclusion, we have presented a realistic optical diffraction tomography experiment that can image three-dimensional objects with a resolution much higher than the one reached with classical microscopes. The superresolution is attained by illuminating the sample with evanescent waves and taking into account the multiple scattering between the objects and the interface in the inversion procedure. We stress that the Born approximation leads to poor results in this configuration and that adding incident propagative waves to the evanescent waves permits one to improve the robustness with respect to noise of the reconstruction.

References

1. J.-J. Greffet and R. Carminati, Prog. Surf. Sci. **56,** 133 (1997).
2. M. Dyba and S. Hell, Phys. Rev. Lett. **88,** 163901 (2002).
3. S. B. Ippolito, B. B. Goldberg, and M. S. Ünlü, Appl. Phys. Lett. **78,** 4071 (2001).
4. O. Haeberlé, A. Dieterlen, and S. Jacquey, Opt. Lett. **26,** 1684 (2001).
5. J. Enderlein, Opt. Lett. **25,** 634 (2000).
6. M. Gustafsson, J. Microsc. **198,** 82 (2000).
7. N. Destouches, C. A. Guérin, M. Lequime, and H. Giovannini, Opt. Commun. **198,** 233 (2001).
8. V. Lauer, J. Microsc. **205,** 165 (2002).
9. E. Wolf, Opt. Commun. **1,** 153 (1969).
10. P. S. Carney and J. C. Schotland, Opt. Lett. **26,** 1072 (2001).
11. K. Belkebir and A. Sentenac, J. Opt. Soc. Am. A **20,** 1223 (2003).
12. P. C. Chaumet, A. Rahmani, F. de Fornel, and J.-P. Dufour, Phys. Rev. B **58,** 2310 (1998).
13. K. Belkebir and A. G. Tijhuis, Inverse Probl. **17,** 1617 (2001).
14. T. M. Habashy, R. W. Groom, and B. R. Spies, J. Appl. Phys. **98,** 1759 (1993).
15. A. G. Tijhuis, K. Belkebir, A. Litman, and B. de Hon, IEEE Trans. Geosci. Remote Sens. **39,** 1316 (2001).